# Pressure-induced phase transitions and metallization in VO$_2$

Ligang Bai,[1,*] Quan Li,[2] Serena A. Corr,[3] Yue Meng,[1] Changyong Park,[1] Stanislav V. Sinogeikin,[1] Changhyun Ko,[4] Junqiao Wu,[4] and Guoyin Shen[1,†]

[1]*High Pressure Collaborative Access Team (HPCAT), Geophysical Laboratory, Carnegie Institute of Washington, Argonne, Illinois 60439, USA*

[2]*College of Materials Science and Engineering and State Key Laboratory of Superhard Materials, Jilin University, Chang Chun 130012, China*

[3]*School of Chemistry, University of Glasgow, Glasgow, United Kingdom*

[4]*Department of Materiasl Science and Engineering, University of California at Berkeley, Berkeley, California 94720, USA*

We report the results of pressure-induced phase transitions and metallization in VO$_2$ based on synchrotron x-ray diffraction, electrical resistivity, and Raman spectroscopy. Our isothermal compression experiments at room temperature and 383 K show that the room temperature monoclinic phase ($M1$, $P2_1/c$) and the high-temperature rutile phase ($R$, $P4_2/mnm$) of VO$_2$ undergo phase transitions to a distorted $M1$ monoclinic phase ($M1'$, $P2_1/c$) above 13.0 GPa and to an orthorhombic phase (CaCl$_2$-like, $Pnnm$) above 13.7 GPa, respectively. Upon further compression, both high-pressure phases transform into a new phase (phase $X$) above 34.3 and 38.3 GPa at room temperature and 383 K, respectively. The room temperature $M1$-$M1'$ phase transition structurally resembles the $R$-CaCl$_2$ phase transition at 383 K, suggesting a second-order displacive type of transition. Contrary to previous studies, our electrical resistivity results, Raman measurements, as well as *ab initio* calculations indicate that the new phase $X$, rather than the $M1'$ phase, is responsible for the metallization under pressure. The metallization mechanism is discussed based on the proposed crystal structure.

PACS number(s): 82.35.Jk, 71.30.+h, 81.40.Vw, 61.05.fm

## I. INTRODUCTION

Transition metal oxides exhibit diverse polymorphism and interesting properties such as metal-insulator transitions (MIT) [1], high-temperature superconductivity [2], and colossal magnetoresistance [3] largely because of the interplay of electronic and lattice degrees of freedom. Significant attention has been given to MIT, which may be triggered by temperature, electric field, pressure, chemical doping, ultrafast laser excitation, and ionizing radiation [4–9]. As was first observed by Morin [10], VO$_2$ undergoes a first-order transition at a modest temperature of 340 K from a high-temperature paramagnetic metallic rutile ($R$) phase to a low-temperature nonmagnetic insulating monoclinic ($M1$) phase. In the $R$ phase (space group $P4_2/mnm$), V ions, nominally V$^{4+}$ in $3d^1$ configuration, are equally spaced along the $c$ axis and located at the center of oxygen octahedra. According to a crystal-field model proposed by Goodenough [11], the 3$d$ orbitals are split into $t_{2g}$ and empty $e_g^\sigma$ orbitals, with $t_{2g}$ further split into an $e_g^\pi$ doublet and an $a_{1g}$ singlet. The $a_{1g}$ orbital with V-V pair bonding is directed along the $c$ axis, and the overlap of $a_{1g}$ and $e_g^\pi$ orbitals in the rutile structure is considered to be responsible for its metallic character. In the $M1$ phase (space group $P2_1/c$), V ions are dimerized and tilted with respect to the $c$ axis, which elevates the $e_g^\pi$ band and splits $a_{1g}$ into bonding and antibonding orbitals, leading to an insulating state. This simple picture is helpful for understanding and interpreting the MIT. However, density functional theory (DFT) calculations did not predict the correct band gap for the $M1$ phase using the experimental structural

data in the absence of strong electron correlations [12,13], suggesting essential roles of electron correlation. Recently, after considering full relaxation of the volume and the atomic structure, the insulating state of the $M1$ phase was predicted by DFT without strong electron correlation [14]. In other words, the MIT in VO$_2$ may be dominantly driven by lattice (or Peierls distortion) [15,16]. From experiments, several researchers claimed that electron-electron correlations cannot be ignored [17]. More recent studies demonstrated that the structural and electronic transitions can be decoupled by temperature [18], pressure [19], and ultrafast laser excitation [20]. It has been also pointed out that the possibility of the MIT may be viewed as a consequence of crystalline distortion rather than a cause of it [21–23]. Despite extensive experimental and theoretical studies, the mechanism of the MIT is still under debate: whether the structural phase transition (Peierls distortion) is the major cause for the temperature driven MIT, or if strong electron correlations (Mott effect) are responsible for opening the band gap of the low-temperature phase.

The application of external pressure provides a unique way to investigate the relationship between structural and electronic properties. It also provides a possible route to decouple the electronic and structural phase transitions. For example, the degree of electron correlation may be changed by tuning the band width under external pressure. Several previous high-pressure studies have been carried out for VO$_2$. The resistivity measurements showed that the transition temperature of the MIT increases linearly up to 4 GPa [22,24]. Recent studies using Raman and infrared spectroscopy techniques showed a phase transition from $M1$ phase to an isostructural phase exhibiting enhanced metallicity above 12 GPa [19,25,26]. An x-ray diffraction (XRD) study under high pressure showed changes in lattice compression of the $b$-$c$ plane of the $M1$ phase, which was considered evidence for the enhanced

*lbai@carnegiescience.edu
†gshen@carnegiescience.edu

metallicity [27]. Because of the isostructural nature of the transition, the authors proposed that the pressure-enhanced metallicity in $VO_2$ is mainly driven by suppressing electron-electron correlation, rather than by the Peierls distortion. However, their data only provided evidence of the metallization process, but lacked direct evidence for a room temperature metallic phase within a monoclinic structure [19]. Also unclear is the role of structural changes (Peierls distortion) in the MIT, and whether the electron correlation alone, tuned by pressure, can induce the MIT. To address these questions, we have studied the pressure effect on structures and electrical resistivity of $VO_2$ up to 55.3 and 61.4 GPa, respectively. We identify that the isostructural phase transition at 13 GPa is a second-order type and is not responsible for metallization. Upon further compression, a high-pressure phase $X$ with monoclinic structure was observed. The Raman and resistivity results indicate that the metallization is achieved in the phase $X$. Its crystal structure is discussed to explain the metallization mechanism.

## II. EXPERIMENTAL PROCEDURES

### A. Sample preparation

Pure single phase $VO_2$ powder samples were used for all the measurements except for the Raman measurements where a single crystal sample was used. The powder samples were prepared in vacuum sealed silica ampoules using a stoichiometric mixture of $V_2O_5$ (99.9%, Alfa Aesar) and $V_2O_3$, with the latter obtained by reduction of $V_2O_5$ in 5% $H_2/N_2$ gas at 900 °C [7]. All experiments were performed in diamond-anvil cells (DAC) with anvils of 300 $\mu$m culet size and rhenium as gasket material.

### B. X-ray diffraction

High-pressure powder XRD measurements were carried out at 16-ID-B and 16-BM-D beamlines of the High Pressure Collaborative Access Team (HPCAT) facility, at the Advanced Photon Source (APS), Argonne National Laboratory (ANL). Two separate isothermal experiments were performed at room temperature and at 383 K up to 55.3 and 53.0 GPa, respectively. Neon was used as pressure-transmitting medium, loaded by using a high-pressure gas-loading system [28]. Pressure was determined by the ruby-fluorescence method [29]. The x-ray beam wavelength was 0.3979 Å. Diffraction patterns were recorded using a MAR3450 imaging plate detector. The intensity versus $2\theta$ patterns were obtained using the FIT2D software [30]. Le Bail whole-profile refinements of the XRD patterns were performed using the FULLPROF software package [31]. Equation-of-state analysis was performed by means of EOSFIT software [32].

### C. Raman spectroscopy

We used the micro-Raman spectrometer at GSECARS sector 13 for Raman measurements. The system is equipped with an argon-ion laser ($\lambda = 514.5$ nm, 50 mW) and a focused spot of diameter 4 $\mu$m at the sample position. A Spec-0.5m spectrograph was used together with an 1800 grooves/mm grating and a liquid nitrogen cooled CCD detector. Neon was

used as pressure-transmitting medium. Similarly, pressure was measured using the ruby fluorescence technique [29].

### D. Resistivity measurements

High-pressure electrical resistivity measurements were performed using the standard four-probe technique in a diamond anvil cell up to 61.4 GPa. A rhenium metal gasket was insulated with a mixture of the epoxy and cubic boron nitride. Four platinum leads were arranged to contact the sample in the chamber. The pressure medium for resistivity measurement was NaCl powder. The resistance was determined by the Van de Pauw method [33]. Pressure was measured using the ruby fluorescence technique [29].

## III. *AB INITIO* CALCULATIONS

We performed DFT calculations with the Vienna Ab-initio Simulation Package (VASP) code [34]. The calculations employed the projector augmented wave (PAW) method and the generalized gradient approximation (PBE-GGA) for electron exchange-correlation interaction [35]. An energy cutoff of 800 eV for the plane-wave expansion and Monkhorst-Pack $k$-point meshes of $10 \times 10 \times 10$ and $7 \times 7 \times 7$ for the rutile and monoclinic structures in the Brillouin zone, respectively, produced enthalpy results well converged to below 1 meV/fu. We had performed systematical tests to evaluate the $U$ values for the GGA$+U$ calculations. All internal atomic coordinates were relaxed until the calculated forces were less than 0.005 eV/Å, and the deviation of the stress tensor from the diagonal hydrostatic form was less than 0.1 GPa. The calculations for the density of states were carried out after the full relaxation of the volume and atomic positions under pressure.

## IV. RESULTS

### A. Pressure-induced structural changes from x-ray diffraction

Typical angle dispersive powder x-ray diffraction data for $VO_2$ at pressures up to 55.3 GPa at room temperature are shown in Fig. 1(a). All the observed diffraction reflections obtained at 1.2 GPa can be indexed with a $M1$ monoclinic structure. The overall $M1$ structure remains unchanged up to 13.0 GPa, above which some of the diffraction peaks start to broaden or split. Despite these changes, the diffraction patterns can still be well indexed with a monoclinic symmetry up to 28.7 GPa with a distorted $M1$ structure of the same space group ($P2_1/c$), which is in general agreement with a previous diffraction study [27]. We refer the distorted phase as $M1'$ because of its similarity to the $M1$ phase.

As pressure was further increased to 34.3 GPa, new diffraction peaks appeared in regions of $2\theta$ between 6° and 9° [Fig. 1(a)]. At 43.1 GPa, the intensity of the peaks from the $M1'$ phase decreases considerably and the new diffraction peaks become dominant at 55.3 GPa. The changes in diffraction peaks clearly indicate a new phase (called phase $X$) starting at 34.3 GPa and both phases ($M1'$, $X$) coexist over a wide pressure range of more than 10 GPa.

Figure 1(b) shows the evolution of x-ray diffraction patterns at elevated temperature of 383 K with increasing pressure.
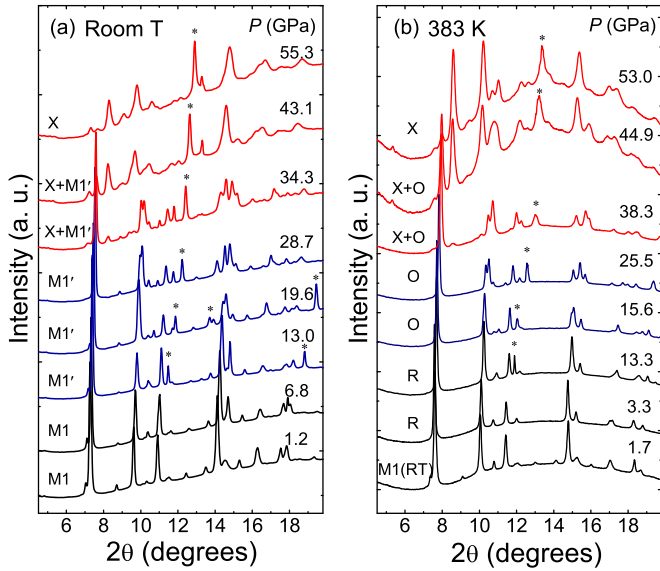
FIG. 1. (Color online) High-pressure x-ray diffraction patterns of VO$_2$ collected at (a) room temperature and (b) 383 K, where $R$ and $O$ denote rutile and CaCl$_2$ phases. The pattern at 1.7 GPa in (b) is collected at room temperature for comparison. Stars indicate diffraction peaks from the Ne pressure medium.
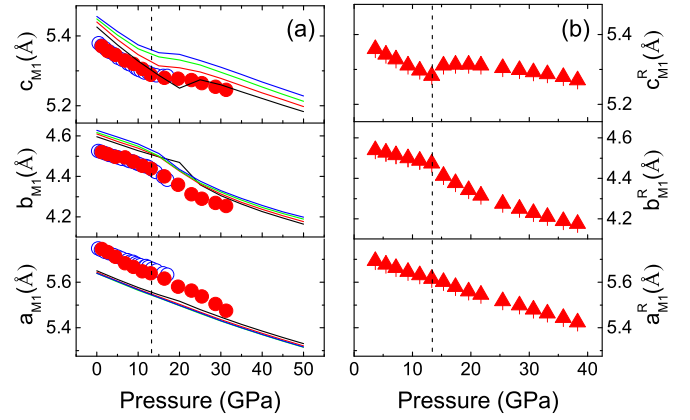


FIG. 2. (Color online) Pressure dependence of $a$, $b$, and $c$ unit cell parameters of the monoclinic structure. Solid red circles are x-ray diffraction data from this study; solid lines are results from *ab initio* GGA+$U$ ($U = 1$ black, 2 red, 3 green, 4 blue; $J = 0.68$) calculations in this study. Open circles are from Ref. [27]. (b) Pressure dependence of unit cell parameters of the rutile and CaCl$_2$ structures. To compare with the compression behavior of monoclinic phases, equivalent lattice parameters ($\boldsymbol{a}_{M1}^R = 2\boldsymbol{c}_R$, $\boldsymbol{b}_{M1}^R = \boldsymbol{a}_R$, $\boldsymbol{c}_{M1}^R = \boldsymbol{a}_R - \boldsymbol{c}_R$) are used.

The first pattern collected at room temperature is the pure $M1$ phase. After heating to 383 K at a pressure of 3.3 GPa, the $M1$ phase transforms to the rutile phase. Above 13.3 GPa, an orthorhombic distortion is obvious from the splitting of $(hkl)$ diffraction lines where $h = k$. This is consistent with the structural distortion from rutile to CaCl$_2$ crystal structures observed in other rutile-type oxides such as CrO$_2$ [36], MnO$_2$ [37], RuO$_2$ [38], and SiO$_2$ [39]. The phase transition from rutile to CaCl$_2$ is a strain-driven, second-order distortive type and proceeds via a rotation of the distorted VO$_6$ octahedra about the $c$ axis. The CaCl$_2$ phase is stable up to 38.3 GPa, above which the diffraction peaks from the phase $X$ appear, similar to those at room temperature. At 53.0 GPa, the phase $X$ becomes the dominant phase.

### B. Pressure dependence of the unit cell parameters and the equations of state

The variations of the unit cell parameters of VO$_2$ with increasing pressure at room temperature and 383 K were obtained by Le Bail whole-profile fitting to each diffraction pattern. Figure 2(a) shows the evolution of the monoclinic lattice parameters as a function of pressure at room temperature, where we compare it with the results of a previous study [27] and our theoretical values calculated within the GGA+$U$ ($U = 1, 2, 3$, and 4). The isostructural phase transition $M1$-$M1'$ at 13 GPa is accompanied by an anomalous compression behavior of the $b$ and $c$ lattice parameters, while the $a$ lattice parameter apparently does not exhibit clear unusual behavior. This is in agreement with previous studies [27].

From theoretical calculations as shown in Fig. 2(a), we find that the effect of $U$ on the compression behavior is relatively large on the $b$-$c$ plane compared to that of the $a$ axis. The overall compression behavior at a given $U$ is almost parallel

to the trends of experimental data. Therefore, $U$ may be not sensitive to pressure.

The structure of the $M1$ phase can be related to that of the high-temperature rutile phase by lattice parameter relations ($\boldsymbol{a}_{M1}^R = 2\boldsymbol{c}_R$, $\boldsymbol{b}_{M1}^R = \boldsymbol{a}_R$, $\boldsymbol{c}_{M1}^R = \boldsymbol{a}_R - \boldsymbol{c}_R$). This notation is used to show the compression of the lattice parameters of the rutile and CaCl$_2$ phases [Fig. 2(b)] for comparison purpose. It is interesting to note that the $R$-CaCl$_2$ transition pressure coincides with that of the $M1$-$M1'$ transition. It can also be seen that the compression behaviors of $M1$ and $M1'$ phases are similar to those of $R$ and CaCl$_2$ phases, indicating that the distortion from $M1$ to $M1'$ phase at ambient temperature is analogous to the transition of rutile to CaCl$_2$ phase at high temperature.

The pressure vs volume data at room temperature and 383 K are plotted in Figs. 3(a) and 3(b) respectively. Equations of states (EOS) are determined by fitting the compression data using the third-order Birch-Murnaghan equation.

$$P = \frac{3B_0}{2}\left[\left(\frac{V_0}{V}\right)^{7/3} - \left(\frac{V_0}{V}\right)^{5/3}\right]$$
$$\times \left\{1 + \frac{3}{4}(B_0' - 4)\left[\left(\frac{V_0}{V}\right)^{2/3} - 1\right]\right\}, \quad (1)$$

where $P$, $V$, and $V_0$ denote pressure, volume at pressure $P$, and volume at ambient pressure, respectively. $B_0$ and $B_0'$ are the zero-pressure bulk modulus and its pressure derivative. The $B_0'$ is fixed to 4 for comparison. As shown in Table I, at room temperature for the $M1$ phase the bulk modulus 213(2) GPa is higher than that for the $M1'$ phase, 167(4) GPa, at 383 K; and 190(2) GPa for the rutile phase is higher than 171(2) GPa for the CaCl$_2$ phase. This is normal for strain-driven distortive-type transition at high pressures. Our data on compression is consistent with the reported data [27] [Fig. 3(a)]. However the
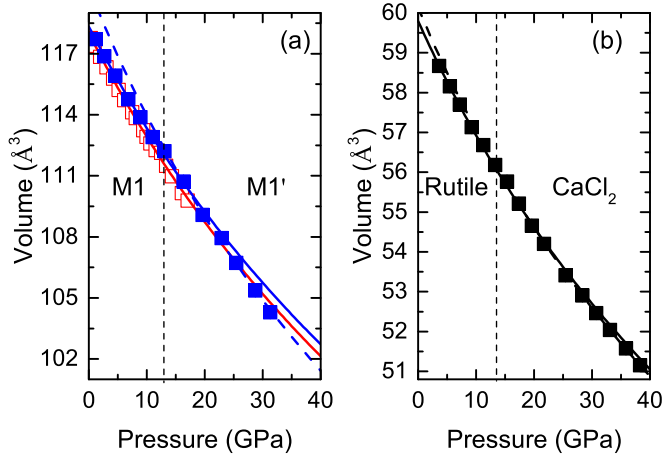
FIG. 3. (Color online) Pressure versus volume data for $VO_2$ at (a) room temperature and (b) 383 K; dashed vertical lines denote transition pressures from (a) $M1$ to $M1'$ phases and (b) rutile to $CaCl_2$ phases. (a) Solid blue squares are data from present XRD; open red squares are previous data from Ref. [15]. The solid and dash blue curves indicate our EOS for M1 and $M1'$ phases respectively, the solid red curves indicate the refitting EOS using data from Ref. [15]. (b) Solid black squares are data from present XRD; the solid and dashed curves indicate our EOS for rutile and $CaCl_2$ phases respectively.

resultant bulk modulus is larger than their value [27], thereby we refit the *P-V* data of Ref. [27], yielding a bulk modulus that is very close to ours.

### C. Pressure dependence of Raman spectra

There are nine Ag and nine Bg Raman active modes in the $M1$ phase of $VO_2$ (space group $P2_1/c$). The measured Raman spectra at high pressures and room temperature are shown in Fig. 4. Ten modes marked as A–J can be identified. With increasing pressure up to 27.8 GPa, all of the Raman peaks shift to higher frequencies. The peak C is broadened and finally splits above 27.8 GPa. It is noted that all the Raman peaks become much weaker above 38.7 GPa and finally disappear above 42.2 GPa. Generally speaking, vanishing of a Raman peak can be accounted for in two ways: (1) a structural transition where no Raman mode is allowed by symmetry, (2) a transition to a metallic state where the Raman signal becomes extremely weak due to the limited penetration depth of the exciting laser. In this case, our XRD results clearly show that the structure in this pressure range cannot be cubic (see below).

TABLE I. Comparison of the EOS parameters for different phases in $VO_2$.

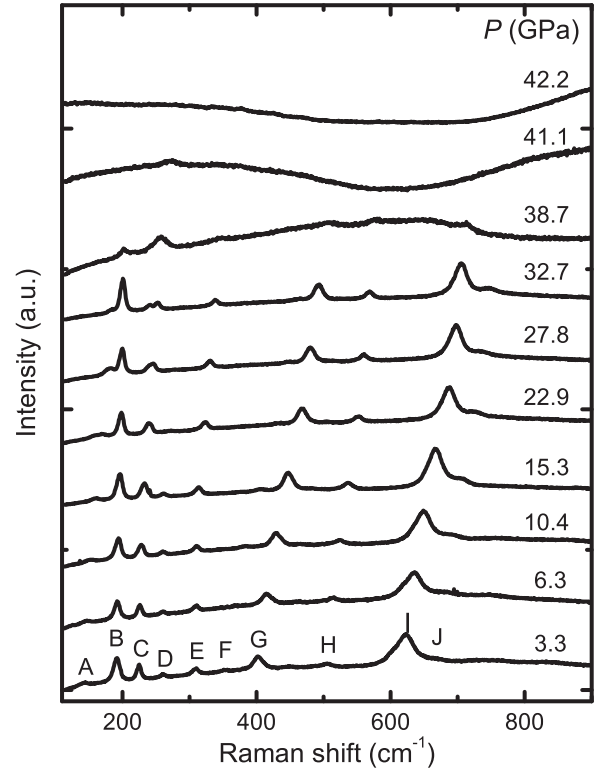| Phase | $V_0$ (Å³) | $B_0$ (GPa) | Reference |
|---|---|---|---|
| $M1$ | 118.32(4) | 213(2) | This study |
| $M1$ | 117.98(4) | 142(1) | Ref. [27] |
| $M1$ | 118.01(1) | 207(3) | Refit Ref. [27] |
| $M1'$ | 120.20(30) | 167(4) | This study |
| Rutile | 59.75(2) | 190(2) | This study |
| $CaCl_2$ | 60.13(6) | 171(2) | This study |



FIG. 4. Raman spectra of $VO_2$ measured at high pressures and ambient temperature. The phonon peaks are labeled by letters from A to J.

So the disappearance of the Raman signal under pressure can be taken as a supporting evidence of metallization.

The pressure dependence of the Raman peaks is plotted in Fig. 5, which can be classified into two regions: 100–350 cm⁻¹ [region 1, Fig. 5(a)] and 350–800 cm⁻¹ [region 2,
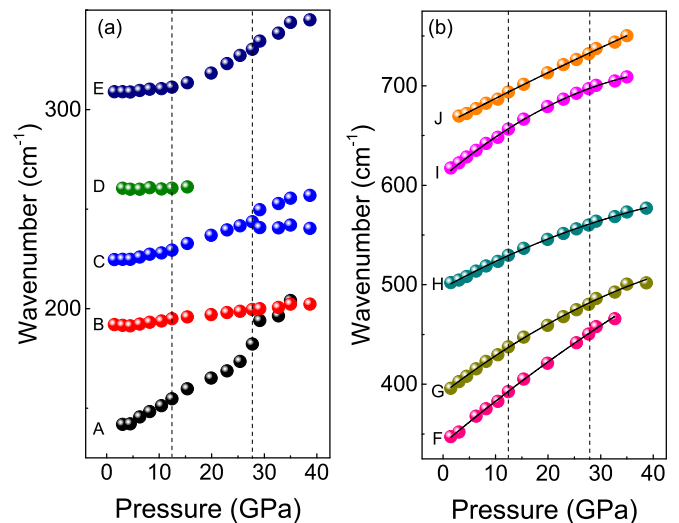


FIG. 5. (Color online) Pressure dependencies of phonon frequencies of $VO_2$ at ambient temperature. Phonon modes from A to J corresponding to those in Fig. 4. (a) Phonon modes between 100 and 350 cm⁻¹, and (b) phonon modes between 350 and 800 cm⁻¹. Changes in Raman peaks are indicated by the vertical dashed lines.
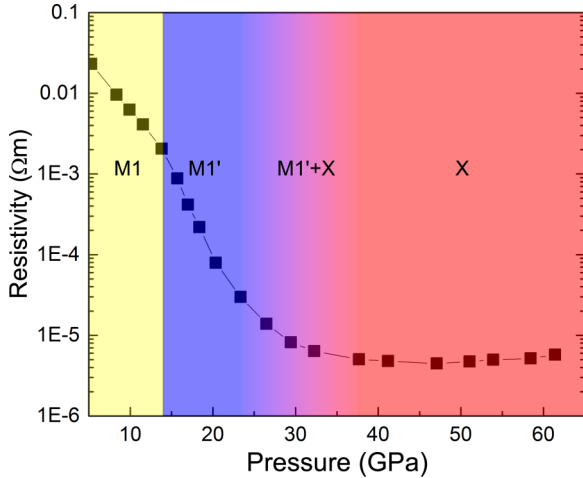
FIG. 6. (Color online) Pressure dependence of electrical resistivity of $VO_2$ at ambient temperature. The transition pressures are indicated by the vertical lines.

Fig. 5(b)]. All the Raman frequencies in region 2 increase smoothly with pressure and can be fitted to a quadratic function of pressure, whereas the Raman frequencies in region 1 display more distinctive features. As shown in Fig. 5(a), the pressure dependences of the Raman shifts can be divided into three subregions indicated by the vertical dashed lines. Below 12.4 GPa, all modes in region 1 (except mode A) shift slightly to higher frequencies with increasing pressure. The lowest mode A shifts to high frequency with pressure faster than other modes, and displays a slight slope change at 12.4 GPa and a jump at 27.8 GPa. Above 12.4 GPa, the B, C, and E modes show rather sharp changes in slope. These observations are in general agreement with the trends reported previously below 19.1 GPa [19]. The slope changes of the B, C, and E modes at 12.4 GPa are related to the phase transition $M1$-$M1'$. Further increasing pressure to above 27.8 GPa leads to the splitting of mode C and discontinuities in the pressure dependencies of other modes, which is related to the appearance of the phase $X$ as observed in XRD.

### D. Electrical resistivity under pressure

Figure 6 presents the electrical resistivity up to 61.4 GPa, determined by using the equation $\rho = (\pi t R / \ln 2)$, where $R$ is the resistance and $t$ is the thickness of the sample [40]. The sample thickness is estimated from the equation of state for $VO_2$ (Table I). The resistivity is 0.02 $\Omega$ m at 5.3 GPa, in the range of reported values of the $M1$ phase [21]. We find a dramatic reduction in resistivity with increasing pressure by more than five orders of magnitude, from $10^{-2}$ $\Omega$ m (at 5.3 GPa) to $10^{-6}$ $\Omega$ m (at 61.4 GPa). A noticeable change in slope was observed at pressure of 14 GPa which is related to the phase transition from $M1$ to $M1'$ at room temperature as observed in our x-ray diffraction and Raman experiments. The resistivity nonlinearly drops with increasing pressure above 23.3 GPa, indicating the start of the phase transition from $M1'$ to $X$. With the pressure increased to greater than 37.7 GPa, the electrical resistivity levels off, and saturates at the level of approximately $\sim 4$–$5 \times 10^{-6}$ $\Omega$ m, which is comparable to
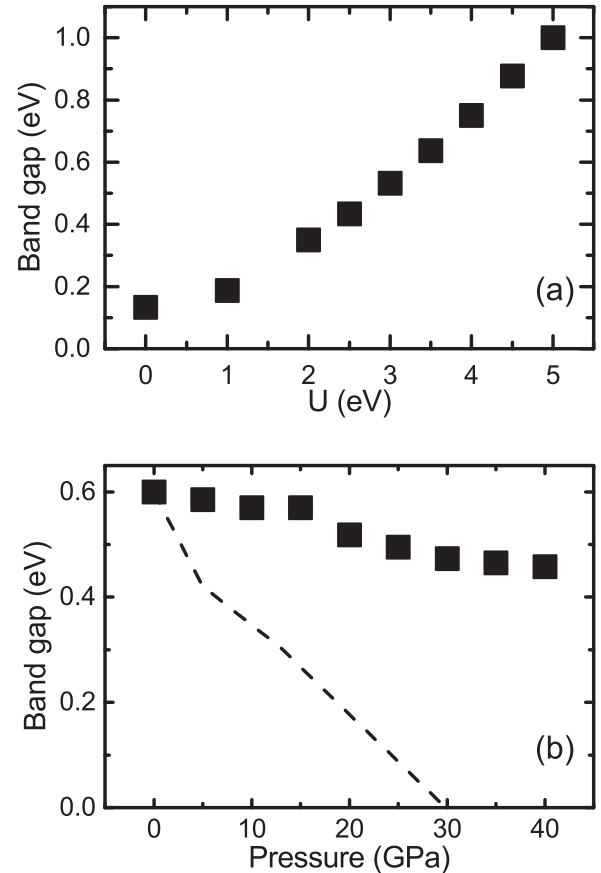


FIG. 7. (a) Band gap $E_g$ as a function of Hubbard parameter $U$. (b) The band gap as a function of pressure (solid squares: calculations; dashed line: deduced from resistivity).

that of metallic rutile $VO_2$ (from $2.3 \times 10^{-6}$ $\Omega$ m at 333 K to $5.0 \times 10^{-6}$ $\Omega$ m at 800 K) [41]. The slightly lower transition pressure from $M1'$ to phase $X$ compared to XRD and Raman results may be due to the different pressure-transmitting media used in our experiments.

### E. Electronic properties from *ab initio* calculations

The dependence of the band gap on electron correlation $U$ for the $M1$ phase of $VO_2$ is shown in Fig, 7(a). It can be seen that there is an open band gap of 0.13 eV at $U = 0$ after full relaxation of atomic positions and lattice parameters. The band gap increases with $U$ almost linearly. The experimental measured band gap ($\sim 0.6$ eV) for the $M1$ phase [42] corresponds to a $U$ value of 3.3 eV, which is not sensitive to pressurization from the results of our structural studies. Figure 7(b) illustrates the two different behaviors of band gap change with pressure in the pressure range from 0 to 40 GPa. We observed a clear change on the slope at the $M1$ to $M1'$ phase transition, however we did not get the closing of the band gap in either $M1$ or $M1'$ phases under pressure.

### V. DISCUSSIONS

The $M1$-$M1'$ phase transition at 13 GPa is associated with anisotropic compression along crystallographic directions, and

can be considered an isostructural transition. This conclusion is consistent with those in previous XRD studies [27]. From comparison with high-temperature phase transition rutile-$CaCl_2$, the $M1'$ structure can be viewed as a monoclinic structure of $CaCl_2$ type and the phase transition $M1$-$M1'$ is likely of second order, so the volume change and atomic displacements at the transition pressure are subtle and continuous. This second-order transition suggests that the rearrangement of V-V chains is unlikely across this transition. This is also supported by the theoretical simulation, which shows that the V-V dimers (Peierls distortion) still exist in the $M1'$ phase.

More importantly this phase transition was believed to be related to an optical gap filling metallization process by Arcangeletti *et al.* based on mid-IR experiments [19]. As shown in Fig. 6, our resistivity results also show a fast decrease with increasing pressure below 30 GPa. The resistivity obeys Arrhenius' law at all pressures: $\rho_0 = A\exp(E_g/2k_BT)$ and $\rho = A\exp(E_g'/2k_BT)$, where $\rho_0$ and $\rho$ are the resistivities at ambient pressure and high pressure respectively, $E_g$ and $E_g'$ are the band gaps at ambient pressure and high pressure respectively, $k_B$ is Boltzmann's constant, and $T$ is temperature. Then at a constant temperature the band gap can be obtained by $\ln(\rho - \rho_0) = (E_g - E_g')/2k_BT$. As shown in Fig. 7(b), the band gap at room temperature derived by the above equation decreases much faster than that from *ab initio* calculations and closes at about 30 GPa, at which $VO_2$ is still in the $M1'$ phase pressure according our XRD and Raman measurements. If the resistivity measurement could reflect the band gap very well, the metallization would occur in the $M1'$ phase under pressure, which would overall agree with previous IR measurements [19]. However, as pointed by Berglund and Guggenheim [21,22], the $VO_2$ samples contain donor- and/or acceptor-like states within the energy gap. Hence, the reduction of activation energy from resistivity measurements and optical gap from mid-IR measurements are largely contributed from the existence of defects, and may not be directly relate to band gap closure. Furthermore, our theoretical calculations show that the correlation effect $U$ is almost constant in the $M1$ and $M1'$ phases and the band gap is not sensitive under hydrostatic pressure. Therefore, pressure does not introduce metallization in the $M1$ and $M1'$ phases, i.e., pressure alone cannot decouple the electronic and the structural transition.

Our XRD results show that the phase transition from $M1'$ to $X$ starts at 34.3 GPa, with the two phases' coexistence spanning over 10 GPa. The Raman and resistivity measurements show similar results. Such a wide coexistence pressure range indicates that this transition is kinetically hindered and first order. Both the disappearance of the Raman signal above 42.2 GPa and the level-off of the resistivity above 37.7 GPa suggest that the phase $X$ is metallic.

The structure of the high-pressure phase $X$ of $VO_2$ at 53 GPa can be indexed with a monoclinic unit cell, $a = 3.586$ Å, $b = 9.686$ Å, $c = 5.207$ Å, $\beta = 94.63°$, $V = 179.73$ Å$^3$, using DICVOL. We consider the transition from rutile to $X$ phase in $VO_2$ to be analogous to those in $TiO_2$ [43] and $NbO_2$ [44] from rutile and distorted-rutile structures to baddeleyite and baddeleyite-related structures at 12.0 and 20.3 GPa, respectively. These transitions are accompanied by the coordination number increase from 6 to 7. In the phase

$X$ of $VO_2$, similarly in $NbO_2$, the oxide anions may occupy a baddeleyite-like arrangement. If we assume $Z = 8$ in phase $X$, the volume change at the transition between $M1'/CaCl_2$ phases and phase $X$ is estimated to be 10%; this compares well with the $\Delta V$ in $TiO_2$ (11.3%) and $NbO_2$ (10.1%). So the phase $X$ is most likely a baddeleyite-related structure, although the detailed structure refinement is not possible due to the insufficient quality of the XRD patterns. Additional evidence of this phase transition is from Raman measurements, since the lowest Raman modes in the rutile phase are related to the rotation of the $MO_6$ ($M$ = metal ion) octahedral around the $z$ axis. So the mode A can be assigned to the octahedral rotation mode. As shown in Fig. 5(a), the mode A only shows a slight slope change in the first phase transition at 12 GPa, which indicates that the $MO_6$ octahedron is stable from $M1$ to $M1'$ phases. In contrast, a sharp change in the second phase transition at 27 GPa was observed, which suggests that the phase $X$ is related to a strengthening of the octahedron induced by the coordination change.

The Raman modes B and C were associated with the paring and tilting motions of V-V dimers by mapping the monoclinic phase onto the tetragonal lattice configuration [25]. The splitting of the mode C above 27.8 GPa then should suggest an activation of the vibration from the new V-V bond in the phase $X$. Actually in the low-pressure Rutile/$M1$ and $CaCl_2$/$M1'$ structures, one-dimensional V-V chains exist through edge-sharing $VO_6$ octahedra along the $c$ axis of the Rutile and $CaCl_2$ structures. In the baddeleyite-related structure phase $X$, each seven-coordinate polyhedral $VO_7$ is edge-sharing with four of them (polyhedra $VO_7$). The unique one-dimensional V-V chains no longer exist. The increase in dimensionality will destroy Peierls distortion and rearrange the V-V bond which will introduce metallization in this high-pressure phase $X$.

## VI. CONCLUSIONS

In summary, the structural, vibrational, and electronic properties of $VO_2$ have been investigated under pressure by a series of experiments and calculations. High-pressure x-ray diffraction measurements performed at room and high temperature show that the $M1$ phase first goes through a displacive distortion above 13.0 GPa at room temperature, which closely resembles the rutile-$CaCl_2$ phase transition above 13.7 GPa at high temperature. The distortion of the $M1$ phase is well reproduced by our *ab initio* calculations. Furthermore, theoretical calculations indicate that there is no metallization in the $M1$ and $M1'$ phases where Peierls distortion exists. Upon further compression to 34.3/38.3 GPa, a new phase transition is observed at room or high temperature. The new phase $X$ can be indexed on a monoclinic unit cell of baddeleyite-like structure. The metallization can only occur in phase $X$ based on our Raman and electrical resistivity measurements. Our experimental and theoretical results suggest that the pressure-induced MIT in $VO_2$ is driven by a structural transition. Further experimental and theoretical studies on the structure of the phase $X$ are necessary to completely characterize the pressure-induced metallization process and to understand the pressure-induced MIT in $VO_2$.

## ACKNOWLEDGMENTS

[1] M. Imada, A. Fujimori, and Y. Tokura, Rev. Mod. Phys. **70**, 1039 (1998).

[2] D. C. Johnston, Adv. Phys. **59**, 803 (2010).

[3] D. N. Basov, R. D. Averitt, D. van der Marel, M. Dressel, and K. Haule, Rev. Mod. Phys. **83**, 471 (2011).

[4] A. Asahara, H. Watanabe, H. Tokoro, S.-i. Ohkoshi, and T. Suemoto, Phys. Rev. B **90**, 014303 (2014).

[5] A. Yamasaki, M. Feldbacher, Y.-F. Yang, O. K. Andersen, and K. Held, Phys. Rev. Lett. **96**, 166401 (2006).

[6] V. Ponnambalam, S. Parashar, A. R. Raju, and C. N. R. Rao, Appl. Phys. Lett. **74**, 206 (1999).

[7] S. A. Corr, D. P. Shoemaker, B. C. Melot, and R. Seshadri, Phys. Rev. Lett. **105**, 056404 (2010).

[8] J. M. Valles, A. E. White, K. T. Short, R. C. Dynes, J. P. Garno, A. F. J. Levi, M. Anzlowar, and K. Baldwin, Phys. Rev. B **39**, 11599 (1989).

[9] K. E. Smith and V. E. Henrich, Phys. Rev. B **50**, 1382 (1994).

[10] F. Morin, Phys. Rev. Lett. **3**, 34 (1959).

[11] J. B. Goodenough, J. Solid State Chem. **3**, 490 (1971).

[12] B.-C. Shih, T. A. Abtew, X. Yuan, W. Zhang, and P. Zhang, Phys. Rev. B **86**, 165124 (2012).

[13] Z. Zhu and U. Schwingenschlögl, Phys. Rev. B **86**, 075149 (2012).

[14] S. Kim, K. Kim, C.-J. Kang, and B. I. Min, Phys. Rev. B **87**, 195106 (2013).

[15] R. M. Wentzcovitch, W. W. Schulz, and P. B. Allen, Phys. Rev. Lett. **72**, 3389 (1994).

[16] V. Eyert, Ann. Phys. (Leipzig) **11**, 650 (2002).

[17] A. Zylbersztejn, Phys. Rev. B **11**, 4383 (1975).

[18] J. Laverock, S. Kittiwatanakul, A. A. Zakharov, Y. R. Niu, B. Chen, S. A. Wolf, J. W. Lu, and K. E. Smith, Phys. Rev. Lett. **113**, 216402 (2014).

[19] E. Arcangeletti, L. Baldassarre, D. Di Castro, S. Lupi, L. Malavasi, C. Marini, A. Perucchi, and P. Postorino, Phys. Rev. Lett. **98**, 196406 (2007).

[20] W.-P. Hsieh, M. Trigo, D. A. Reis, G. Andrea Artioli, L. Malavasi, and W. L. Mao, Appl. Phys. Lett. **104**, 021917 (2014).

[21] C. Berglund and H. Guggenheim, Phys. Rev. **185**, 1022 (1969).

[22] C. Berglund and A. Jayaraman, Phys. Rev. **185**, 1034 (1969).

[23] A. Cavalleri, T. Dekorsy, H. H. W. Chong, J. C. Kieffer, and R. W. Schoenlein, Phys. Rev. B **70**, 161102 (2004).

[24] C. H. Neuman, A. W. Lawson, and R. F. Brown, J. Chem. Phys. **41**, 1591 (1964).

[25] C. Marini, E. Arcangeletti, D. Di Castro, L. Baldassare, A. Perucchi, S. Lupi, L. Malavasi, L. Boeri, E. Pomjakushina, K. Conder, and P. Postorino, Phys. Rev. B **77**, 235111 (2008).

[26] C. Marini, L. Baldassarre, M. Baldini, A. Perucchi, D. Di Castro, L. Malavasi, S. Lupi, and P. Postorino, High Press. Res. **30**, 55 (2010).

[27] M. Mitrano, B. Maroni, C. Marini, M. Hanfland, B. Joseph, P. Postorino, and L. Malavasi, Phys. Rev. B **85**, 184108 (2012).

[28] M. Rivers, V. B. Prakapenka, A. Kubo, C. Pullins, C. M. Holl, and S. D. Jacobsen, High Press. Res. **28**, 273 (2008).

[29] H. K. Mao, J. Xu, and P. M. Bell, J. Geophys. Res. **91**, 4673 (1986).

[30] A. P. Hammersley, S. O. Svensson, M. Hanfland, A. N. Fitch, and D. Hausermann, High Press. Res. **14**, 235 (1996).

[31] J. Rodríguez-Carvajal, Physica B (Amsterdam) **192**, 55 (1993).

[32] R. J. Angel, Rev. Mineral. Geochem. **41**, 35 (2001).

[33] L. J. van der Pauw, Philips Res. Rep. **13**, 1 (1958).

[34] G. Kresse and J. Furthmuller, Phys. Rev. B **54**, 11169 (1996).

[35] J. P. Perdew, K. Burke, and M. Ernzerhof, Phys. Rev. Lett. **77**, 3865 (1996).

[36] B. R. Maddox, C. S. Yoo, D. Kasinathan, W. E. Pickett, and R. T. Scalettar, Phys. Rev. B **73**, 144111 (2006).

[37] J. Haines, J. Léger, and S. Hoyau, J. Phys. Chem. Solids **56**, 965 (1995).

[38] J. Haines and J. M. Léger, Phys. Rev. B **48**, 13344 (1993).

[39] K. J. Kingma, R. E. Cohen, R. J. Hemley, and H.-k. Mao, Nature (London) **374**, 243 (1995).

[40] X. Huang, C. Gao, Y. Han, M. Li, C. He, A. Hao, D. Zhang, C. Yu, G. Zou, and Y. Ma, Appl. Phys. Lett. **90**, 242102 (2007).

[41] P. B. Allen, R. M. Wentzcovitch, W. W. Schulz, and P. C. Canfield, Phys. Rev. B **48**, 4359 (1993).

[42] H. Verleur, A. Barker, and C. Berglund, Phys. Rev. **172**, 788 (1968).

[43] L. Gerward and J. Staun Olsen, J. Appl. Crystallogr. **30**, 259 (1997).

[44] J. Haines, J. M. Léger, A. S. Pereira, D. Häusermann, and M. Hanfland, Phys. Rev. B **59**, 13650 (1999).